Improved Main-Beam Nulling Through Single Switchable Displaced Element for Small Scale Adaptive Array

Han Wang, Zhijun Zhang, *Senior Member, IEEE*, Yue Li, *Member, IEEE*, and Zhenghe Feng, *Fellow, IEEE*

***Abstract*—This paper proposes a novel scheme to improve the signal-to-noise ratio (SNR) response of the main beam nulling for small-scale adaptive arrays. This method effectively promotes the main-beam nulling performance by introducing a displaced element at the end of an adaptive array. It is easy to implement with very low system cost. A detailed analysis of its working mechanism is provided, and the performance is verified with the simulation results. A switching scheme is introduced further to realize consistent performance for all nulling regions, which can attain similar main beam nulling performance as a larger-scale adaptive array. Combining with the active element pattern method, the performance of the proposed scheme involving mutual coupling is examined with a dipole array. It is consistent with the results acquired in isolated condition, which verifies its feasibility in practice.**

***Index Terms*—Adaptive array, interference cancellation, mutual coupling, smart antenna.**

I. Introduction

AMONG many anti-interference schemes proposed for wireless communication systems, the adaptive array is one of the most prominent techniques because it is based on the untapped space resources. By utilizing its controllable radiating elements, it can act as a space filter to dynamically form a beam to aim at the direction of signal and cancel the interference with its null. Thus, it can provide gain to the output SNR and realize interference rejection when comparing with the omnidirectional antennas.

Traditionally, the adaptive array is mainly based on the uniformly spaced array, and the synthesis algorithms, such as Applebaum's maximize signal-to-noise and interference ratio (MSINR) algorithms [1] and Widrow's least mean square error (LMS) algorithms [2], are developed to calculate the optimal weighting factors. To estimate the arriving angles of the signal and interference, related direction of arrival (DOA) estimation techniques are developed; and spectral estimation methods, including super resolution algorithms [3], maximum likelihood method [4], and MUSIC [5], are introduced to achieve better convergence speed and higher resolution. However, advances in the system performance related to array itself are rarely reported. Some known works beyond the algorithmic aspect may include the only phase/amplitude/position adjustable array to reduce the system complexity [6]–[8] and perturbation in the position and phase of an array to improve the accuracy of nulling [9].

By studying these literatures above, it can be noticed that most of them are based on large-scale arrays that contains tens to hundreds of elements. These arrays are designed for military applications and can provide considerable gain with sufficient flexibility in interference cancellation. Their beams are narrow and the interference would mostly locate in the side-lobe area. Consequently, the main beam interference is not a serious problem in these cases.

However, such performance is acquired at the expense of high system cost, complexity and power consumption. The convergence speed of adaptive algorithm is also related to the amount of elements [10], which requires sufficient system processing capability. Therefore, the large scale array is only applicable in specific application scenarios.

Some simplified adaptive systems, namely partially adaptive array [11] and side lobe canceller (SLC) [12], are investigated to realize nulling in a fixed main beam. Even though the complexity is effectively controlled by reducing the usage of adaptive elements, the size is still too large and the performance is sacrificed because only the auxiliary array is adaptive, which cannot contribute to overall performance.

Attracted by the unique features of the adaptive array, newly appeared applications such as multiple nodes wireless ad-hoc network have gradually adopted this technique [13]. In this case, the large-scale fully adaptive array cannot be applied in all nodes due to the limitations in cost, volume and complexity. Meanwhile, the digital beam forming devices installed on mobile carriers (vehicle, etc.) have limited computational capability. Thus, small-scale adaptive arrays, say less than eight elements, are better suited to these applications. However, the main beam of the small-scale adaptive array is much wider than the larger-scale one. It raises a serious challenge considering the high possibility of the interference falling into the main beam region, which will result in significant performance deterioration.

To meet this challenge, a novel scheme is proposed in this paper to improve the output SNR response of the small-scale array when the interference falls into the main beam region. Section II provides a detailed analysis of its working mechanism, which is easy to implement without increasing the system

Manuscript received May 27, 2012; revised December 14, 2013; accepted February 01, 2014. Date of publication February 20, 2014; date of current version May 01, 2014. This work was supported by the National Basic Research Program of China under Contract 2013CB329002, in part by the National High Technology Research and Development Program of China (863 Program) under Contract 2011AA010202, the National Natural Science Foundation of China under Contract 61271135, the China Postdoctoral Science Foundation funded project 2013M530046, the National Science and Technology Major Project of the Ministry of Science and Technology of China 2013ZX03003008-002.

The authors are with the State Key Laboratory of Microwave and Communications, Tsinghua National Laboratory for Information Science and Technology, Tsinghua University, Beijing 100084, China (e-mail: zjzh@tsinghua.edu.cn).

Digital Object Identifier 10.1109/TAP.2014.2307326

complexity. The simulation results are presented in Section III with comparisons to the uniformly spaced array, which demonstrate better main beam nulling performance in all cases. To enhance the global performance for all nulling regions, a switching scheme is introduced in Section IV. The proposed switchable array can achieve nulling performance similar to a larger-scale array in the main beam region. Meanwhile, it can maintain consistent performance as a uniformly spaced array in the side lobe region. Finally, the performance of the proposed scheme in the real scene is examined with a dipole array in Section V. Mutual coupling effect is taken into consideration where the active element pattern method is adopted to calculate the weighting factor and pattern. The result confirms that the proposed scheme is still effective when involving mutual coupling, which verifies its feasibility in practice. Considering that the signal-to-interference ratio (SIR) is good and similar in all cases, the output SNR is adopted as an evaluation criterion to compare the performance throughout this paper.

II. Array Structure And Analysis

In traditional analysis of the uniformly spaced adaptive array, Applebaum algorithm [1] can adjust the nulling position to acquire good interference rejection by sensing the correlation between noise, interference and signal. It is assumed that every element in an array is omnidirectional and isolated from others. The desired signal and the jammer are presented as an individual plane wave from θ_d, θ_j, which can be described using the receiving vector provided in (1)

$$S = i_s(t)b_d = i_s(t)\begin{bmatrix} 1 \\ e^{jkd_1\cos\theta_d} \\ \vdots \\ e^{jkd_{N-1}\cos\theta_d} \end{bmatrix}$$
$$J = i_j(t)b_j = i_j(t)\begin{bmatrix} 1 \\ e^{jkd_1\cos\theta_j} \\ \vdots \\ e^{jkd_{N-1}\cos\theta_j} \end{bmatrix}. \quad (1)$$

In (1), k denotes the free space wave vector; d_i gives the distance of ith element from the origin; $i_s(t), i_j(t)$ represent the amplitude of the signal and jammer, and b_d, b_j indicate the direction vector of the signal and jammer.

The noise in this analysis is assumed to be uncorrelated Gaussian white noise with equal variance σ_n for all elements. And the covariance matrix for both the jammer and the noise are given in (2), as shown at the bottom of the page, where $\sigma_j^2 = \overline{|i_j(t)|^2}$ denotes the variance of the jammer. Accordingly, the Applebaum's weighting factors W_{opt} can be calculated with (3), where $(\cdot)^*$ denotes the complex conjugate of a given vector

$$W_{\text{opt}} = (R_{\text{nn}} + R_{\text{jj}})^{-1} b_d^*. \quad (3)$$

The synthesis pattern $f(\theta)$ can be given by (4) with the information given above, where $(\cdot)^T$ denotes the transpose of a given vector

$$f(\theta) = b^T W_{\text{opt}} = \begin{bmatrix} 1 \\ e^{jkd_1\cos\theta} \\ \vdots \\ e^{jkd_{N-1}\cos\theta} \end{bmatrix}^T W_{\text{opt}}. \quad (4)$$

It can be noticed that R_{nn} is a diagonal matrix and R_{jj} is a Hermitian matrix of order N, the inverse result for $R_{\text{nn}} + R_{\text{jj}}$ can be expanded and divided into two parts as (5)

$$(R_{\text{nn}} + R_{\text{jj}})^{-1} = R_{\text{nn}}^{-1} - \frac{\sigma_j^2}{\sigma_n^2\left(\sigma_n^2 + N\sigma_j^2\right)} R_{\text{jj}}. \quad (5)$$

Consequently, pattern function (4) can be rewritten as (6), where the synthesis pattern is divided into two parts [1]

$$\begin{aligned} f(\theta) &= b^T R_{\text{nn}}^{-1} b_d^* - \frac{\sigma_j^2}{\sigma_n^2\left(\sigma_n^2 + N\sigma_j^2\right)} b^T R_{\text{jj}} b_d^* \\ &= f_q(\theta) - f_c(\theta). \end{aligned} \quad (6)$$

To gain a better understanding of the nulling process, these two parts are named as the quiescent pattern $f_q(\theta)$ and the cancellation pattern $f_c(\theta)$. The former one aims at providing the max SNR response without interference, where the beam is pointing to the direction of signal. The latter one is generated to realize interference nulling, whose pattern would steer to the interference direction and impose the cancellation in a proper extent. Fig. 1 demonstrates these three patterns $f(\theta)$, $f_q(\theta)$ and $f_c(\theta)$ together in one figure with the interferences coming from different angles.

As can be seen in this figure, when the interference is located in the side lobe area as shown in Fig. 1(a), the amplitude of $f_c(\theta)$ is quite low and the nulling process has slight effect on the main beam. However, when the interference gets into the main beam region as shown in Fig. 1(b), the amplitude of $f_c(\theta)$ is comparable to the peak value for $f_q(\theta)$, which means the nulling effect on the main beams cannot be ignored anymore. The synthesized pattern splits, and a considerable gain loss in the direction of signal can be observed in this case. This scenario, namely the main beam nulling, is quite common in the small-scale arrays because its main beam is much wider than the large-scale array.

$$R_{\text{nn}} = \sigma_n^2 \begin{bmatrix} 1 & & 0 \\ & \ddots & \\ 0 & & 1 \end{bmatrix}$$
$$R_{\text{jj}} = \sigma_j^2 \begin{bmatrix} 1 & e^{-jkd_1\cos\theta_j} & \cdots & e^{-jkd_{N-1}\cos\theta_j} \\ e^{-jkd_1\cos\theta_j} & 1 & \cdots & e^{-jkd_{N-2}\cos\theta_j} \\ \vdots & \vdots & \ddots & \vdots \\ e^{-jkd_{N-1}\cos\theta_j} & e^{-jkd_{N-2}\cos\theta_j} & \cdots & 1 \end{bmatrix} \quad (2)$$

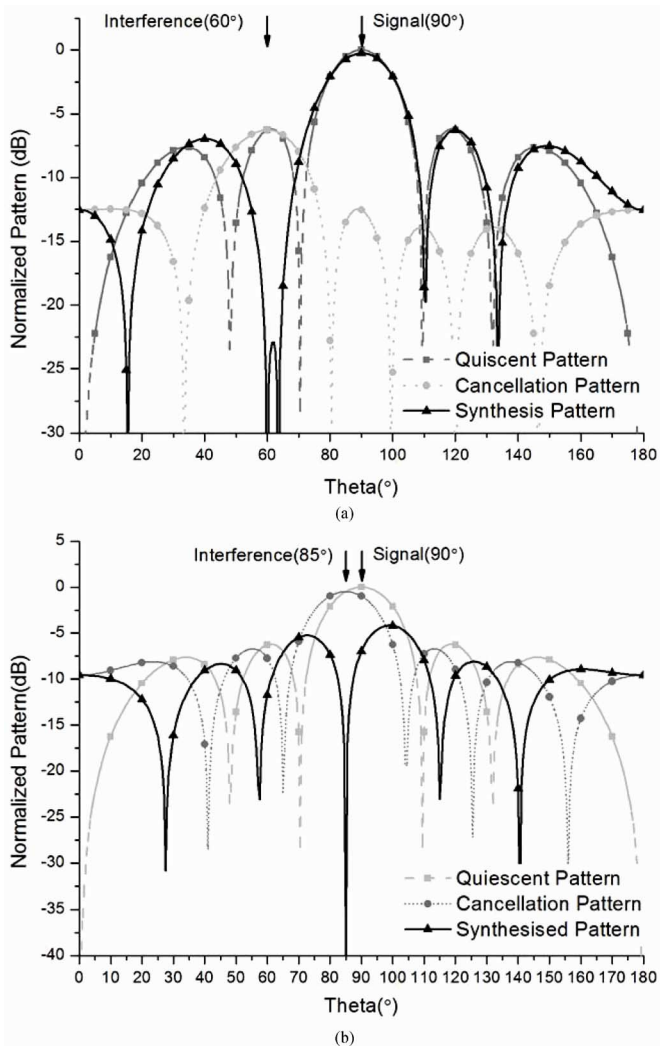

Fig. 1. Two different situations for interference nulling in small scale array: (a) side lobe nulling and (b) main beam nulling.

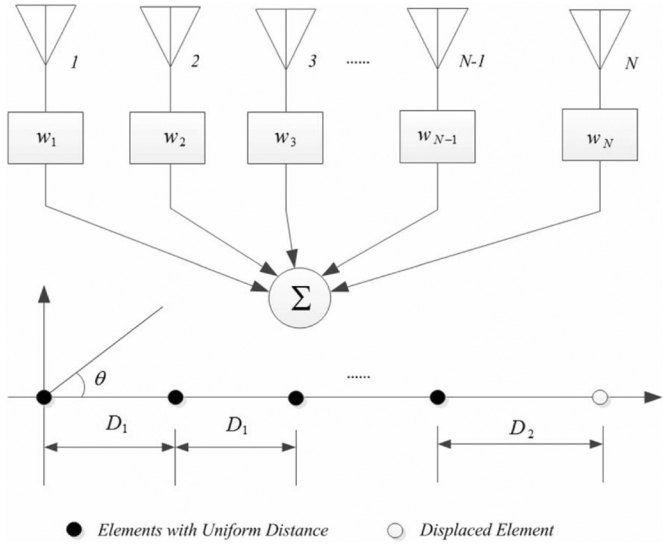

Fig. 2. System diagram and the structure of the proposed array.

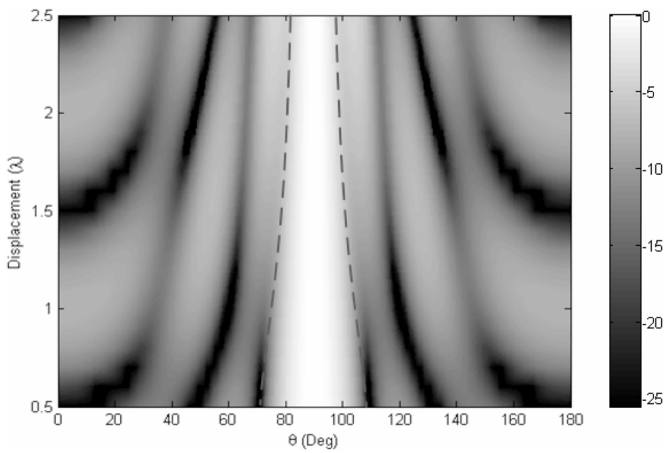

Fig. 3. Normalized pattern of $F(\theta, \theta_r)$ at different displacement.

Although the SIR is still good in this case, the output SNR will degrade into an unacceptable level due to the severe degradation in antenna gain. Thus, the main beam nulling performance is critical for the small scale array; and the output SNR is used as a criterion to evaluate the main beam nulling performance in all discussions throughout this paper.

To solve this problem, a better resolution and roll-off character are in demand for the small-scale adaptive array. By examining the pattern function provided in (6), the quiescent pattern $f_q(\theta)$ and the cancellation pattern $f_c(\theta)$ can be rewritten as (7)

$$f_q(\theta) = \frac{1}{\sigma_n^2} F(\theta, \theta_d)$$
$$f_c(\theta) = f_q(\theta_j) \frac{\sigma_j^2}{\sigma_n^2 + N\sigma_j^2} F(\theta, \theta_j) \tag{7}$$

and the same factor $F(\theta, \theta_r)$, as shown in (8), can be collected for both patterns, where θ is the function variable and θ_r is the constant reference angle (either to be θ_d or θ_j)

$$F(\theta, \theta_r) = \sum_{i=1}^{N} e^{jkd_i(\cos\theta - \cos\theta_r)}. \tag{8}$$

In this function, since N is determined by the array size, only d_i value or the separation between adjacent elements can be adjusted to acquire a desired roll-off character.

Equally increasing the distance between elements is one solution; however, the grating lobe would appear when the distance comes close to or greater than λ, which is unacceptable in real communication circumstance. Consequently, a partial displaced method is proposed in this paper, whose elements distribution is depicted in Fig. 2. It is still based on an N elements fully adaptive array, in which the outermost element spaces D_2 from others while all other elements are uniformly spaced with D_1 $(\lambda/2)$. Since only one element is displaced from all others, the main beam is mainly determined by a central $N-1$ element, and the displaced element would not generate a grating lobe but perform a shaping on the main beam. To evaluate the effectiveness of the proposed scheme, Fig. 3 gives the relationship between the common factor $F(\theta, \theta_r)$ and the displacement D_2 $(\theta_r = 90°, N = 6)$, which is calculated by (9)

$$F(\theta, \theta_r)_{\text{pattern}} = 10\log[F^*(\theta, \theta_r)F(\theta, \theta_r)]. \tag{9}$$

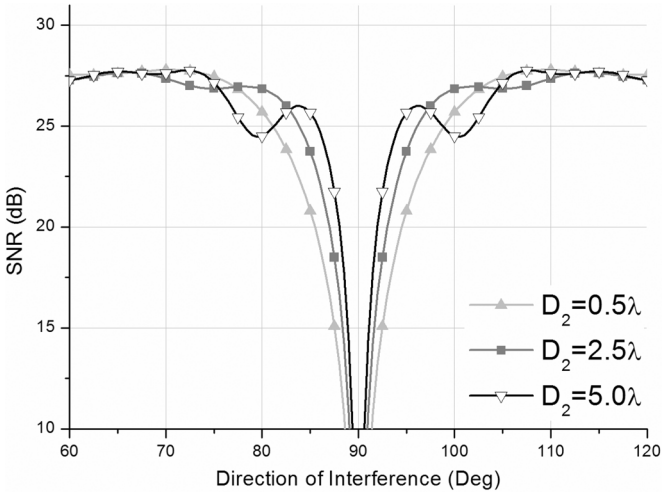

Fig. 4. SNR-θ_j curve at different displacement, $N = 6$.

It can be noticed that the main beam width for, which is the white area within the dash line, shrinks from 40° to 20° by increasing the displacement of the outmost element from 0.5λ to 2.5λ. It means a better roll-off character or nulling performance is acquired with this proposed method.

III. Simulation Results

To verify the previous analysis, the output SNR, which is calculated by (10), is simulated for different displacement D_2

$$\mathrm{SNR} = \frac{(W_{\mathrm{opt}}^* S^*)(S W_{\mathrm{opt}})}{W_{\mathrm{opt}}^* R_{\mathrm{nn}} W_{\mathrm{opt}}}. \tag{10}$$

The simulation is undertaken in Matlab environment, and the input SNR, SIR ratio is set as (11), which simulates a strong interference at moderate noise condition.

$$\mathrm{SNR}_{\mathrm{input}} = \frac{\overline{|i_s(t)^2|}}{\sigma_n^2} = 20 \text{ dB}$$
$$\mathrm{SIR}_{\mathrm{input}} = \frac{\overline{|i_s(t)^2|}}{\sigma_j^2} = -20 \text{ dB}. \tag{11}$$

Besides, N is selected as 4, 6, 8 as a small-scale array, where the direction of signal is set to $\theta_d = 90°$ and the interference is injected within $\pm 30°$ that covers the main-beam area.

An example of the SNR-θ_j curve is depicted in Fig. 4 for $N = 6$. There are three different displacements from 0.5λ to 5λ. It can be observed that all three curves show a decline in the output SNR when the interference is getting close to the signal, but the roll-off character varies with different displacements. When the interference approaches the signal, a sharper roll-off can be acquired with larger D_2, which means better main beam nulling performance is acquired with the proposed scheme. However, a pit area emerged around $\theta_d = 81°, 99°$ for the $D_2 = 5\lambda$ curve, whose formation mechanism and solution will be discussed in Section IV.

To evaluate the performance for all cases, Fig. 5 gives the relationship of the output SNR improvement to the displacement D_2 with the interference coming from different θ_j. This surface is acquired by subtracting the result of $D_2 = 0.5\lambda$ from the one of $D_2 > 0.5\lambda$; and the $\mathrm{SNR} < 20$ dB area is discarded with a cut surface around θ_d. The D_2 is selected from uniform 0.5λ to displaced 5.0λ and the direction of signal θ_d is chosen as 90°.

From left to right, these three figures represent the 4, 6, and 8 elements cases. It can be noted that this proposed method is very effective in small-scale arrays. The SIR is better than 50 dB for all cases. Around 12 dB increments is acquired at $D_2 = 5\lambda$, $N = 4$ condition; and the $\mathrm{SNR} < 20$ dB area also constrains to provide an extended nulling range. However, when the number of elements increases, the improvement in the output SNR decreases from 12 to 6 dB, which can be explained by the lowered contribution of a single element to the whole array.

IV. Switching Scheme

From the result given in the previous section, better output SNR performance of the main beam nulling is acquired by increasing D_2 without adding system complexity. However, as mentioned in Section III, unlike a uniformly spaced array, the output SNR of the proposed array is not a monotone function when the interference moves away from the main beam. As shown in Fig. 4, the output SNR degrades around $\theta_d = 81°, 99°$ for $N = 6, D_2 = 5\lambda$.

To analyze this phenomenon, patterns at the pit point ($\theta_j = 81°$) and the maximal point ($\theta_j = 85°$) are given in Fig. 6, which plots the quiescent pattern and the cancellation pattern together. As can be observed in this figure, the quiescent pattern and the cancellation pattern for both points share the same shape but different amplitude, which is in accordance with (8). Since D_2 is larger than λ, the shaping effect introduced by this displaced element not only affects the peak area but also the adjacent one. Amplitude vibrations can be observed in the pattern which is similar to a high order modulation applied on the pattern. Even though the beam width of the central peak narrows to achieve a better roll-off character, two adjacent peaks converge to the central area which induce different impacts on the direction of signal when changing the direction of the jammer. As shown in Fig. 6(a), the adjacent peak of the cancellation pattern is aligned with the direction of signal when the interference is located at 81°, thus the gain and the output SNR are impaired to a large extent (5 dB in this case). Comparatively, when the interference is set at 85° as shown in Fig. 6(b), this adjacent peak of cancellation pattern shifts away from the signal direction, thus the impact on the synthesized pattern is only 2 dB. Consequently, the output SNR not increase monotonously when the interference moves toward the side lobe area as shown in Fig. 4.

To obtain overall improvement in the output SNR for all nulling regions, a switching scheme is introduced as shown in Fig. 7. The array contains $N + 1$ elements but only N weighting units. The $N + 1$th element is displaced D_2 from other N equally spaced $(\lambda/2)$ elements. An RF switch is used to switch between the Nth and the $N + 1$th element, which can swap the array between a N-element uniform state and a N-element displaced state. The switching criteria adopted in this scheme is similar to the selection combining technique used in a diversity combining system, which would choose the path that yields the better output SNR. With this scheme, the array not only attains a sharper roll-off in the main beam area, but also acquires a flat response in the side lobe area.

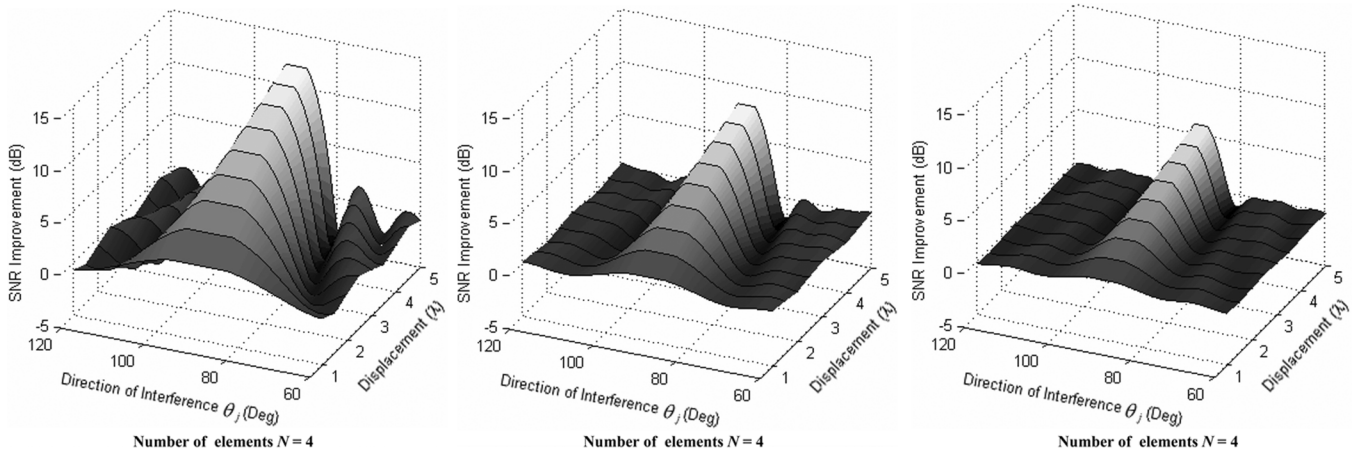

Fig. 5. Improvement of output SNR and its relationship to the direction of interference θ_j and the displacement $D_2(\theta_d = 90°)$.

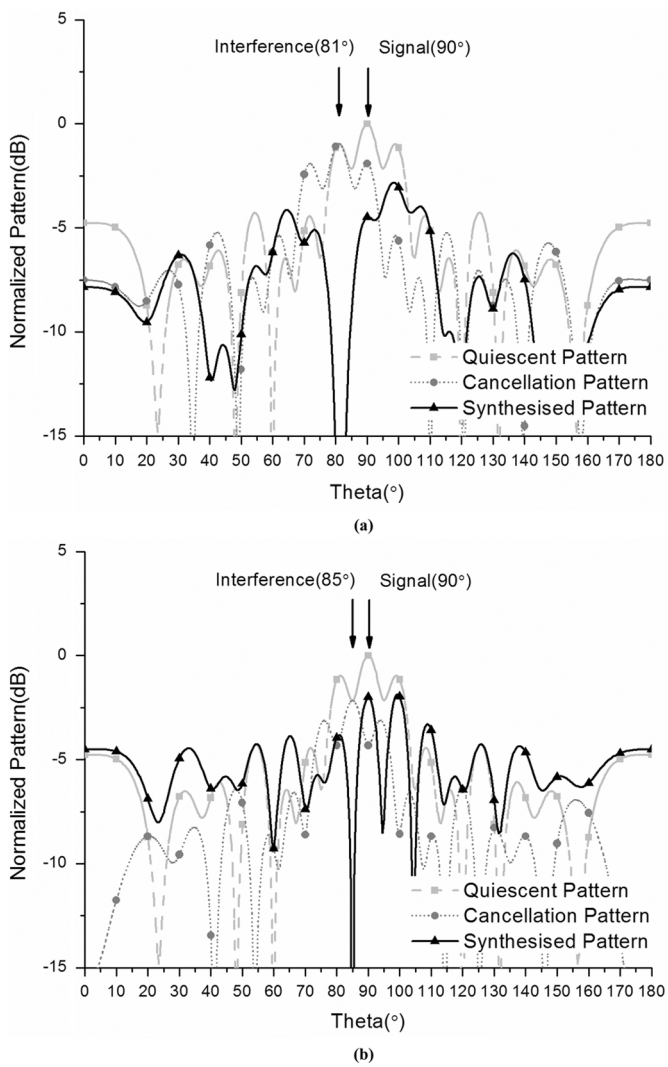

Fig. 6. The quiescent, cancellation and synthesis patterns in (a) $\theta_j = 81°$ (b) $\theta_j = 85°$ at $N = 6$, $D_2 = 5\lambda$ condition.

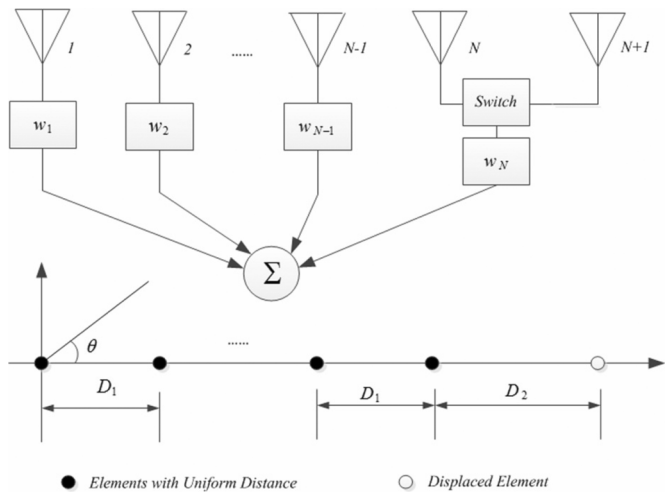

Fig. 7. System diagram and the structure of the proposed array with switching scheme.

To demonstrate the effectiveness of this switching scheme, the SNR-θ_j curves with/without switching for $N = 4$ and $N = 6$ cases are provided in Fig. 8. In order to verify that it has similar performance with the signal coming from different angles, curves for $\theta_d = 60°$ and $\theta_d = 90°$ are provided. Refer to Fig. 8(a), the dashed line with circular markers exhibits the nulling performance of a four-element uniformly spaced array; the dash line with square symbols gives the nulling performance of a four-element displaced array; and the dot line with triangle markers denotes the performance of a ten-element uniformly spaced array as reference. In the side lobe area, it can be observed that the output SNR of the uniformly spaced arrays tends to be stable when the interference moves away from the direction of signal. Comparatively, the output SNR of the displaced array starts to oscillate, which is undesirable in application. Since a ten-element array has around 4 dB higher gain in theory when comparing with a four-element array, the output SNR of the ten-element reference array is also 4 dB higher than the four-element array in the side lobe area when is smaller than 65° or larger than 115°. In the main beam area, the output SNR of the uniform four-element array degrades monotonously and much faster than the ten-element array. Comparatively, the result of the four-element displaced array exhibits a very sharp roll-off around the direction of the signal. The SNR-curve almost overlaps with the $N = 10$ reference array in the roll-off

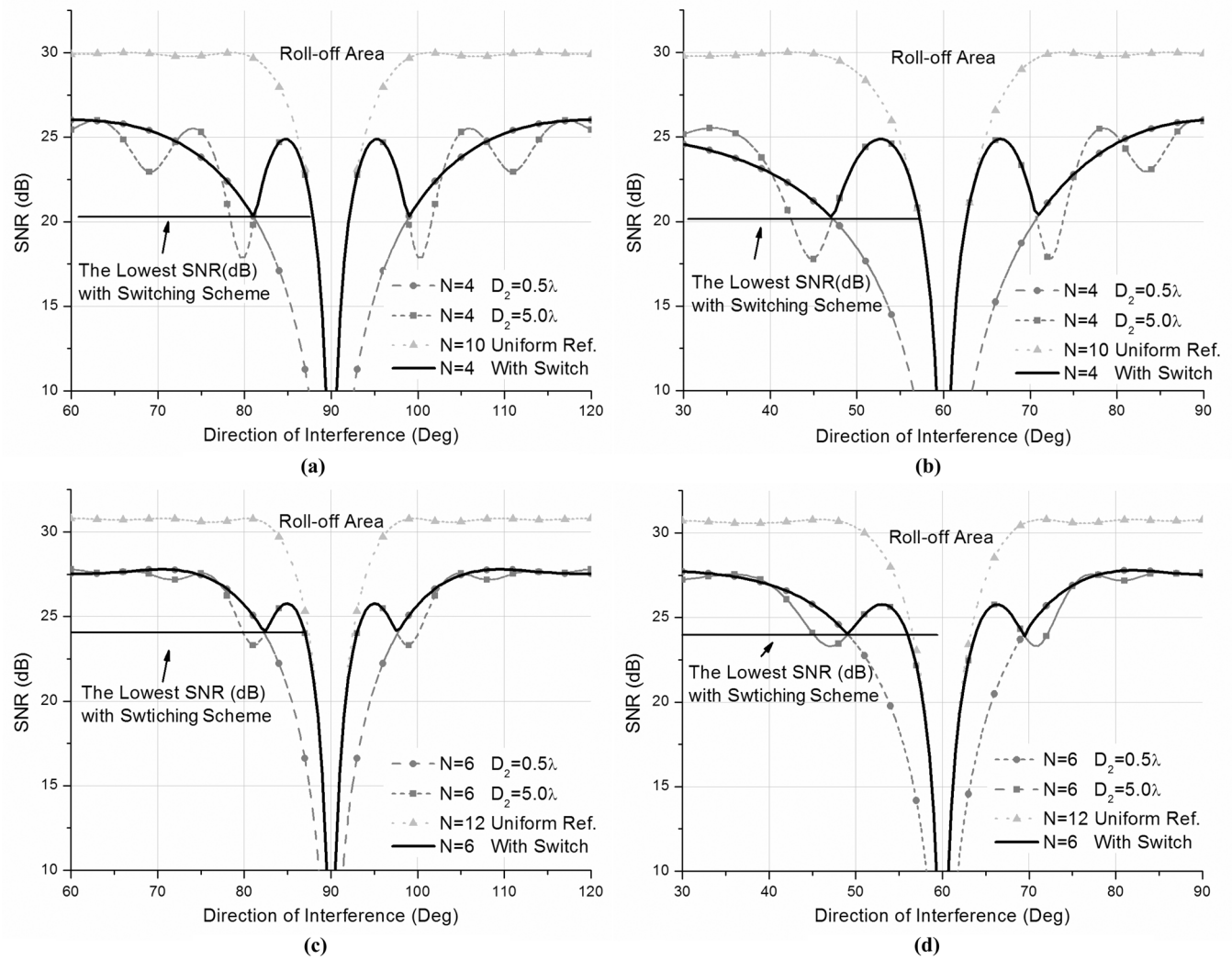

Fig. 8. Switching scheme and its performance when (a) $N = 4$, $\theta_d = 90°$, (b) $N = 4$, $\theta_d = 60°$, (c) $N = 6$, $\theta_d = 90°$, (d) $N = 6$, $\theta_d = 60°$.

area, which proves that the four-element displaced array has similar main beam nulling capability as a ten-element uniformly spaced array. By adopting the switching scheme, the merits of both the uniformly spaced and displaced arrays merge together. The solid line in Fig. 8(a) represents the result, which has a stable output in the side lobe area along with a sharper roll-off in the main beam region. The similar phenomena can also be observed in all cases as shown in Fig. 8(b)–(d).

In practice, the switching condition between the uniform state and the displaced state of the array can be chosen as the intersection point of their SNR-curves, or the lowest output SNR point as shown in Fig. 8. Since the complexity of the RF switch is much lower than the weighting unit, this system is more cost effective than a large-scale adaptive array but with similar main beam nulling performance.

V. Performance Verification Involving Mutual Coupling

In previous analysis, the amelioration in the output SNR validated the effectiveness of the proposed scheme. For analytical convenience, all the elements are presumed to be isotropic and no mutual coupling is considered in the study. However, this presumption may not be tenable for all scenarios. The elements might be closely placed and the mutual coupling between elements may be strong.

In this section, to verify the performance of the proposed scheme in a real scene, we examine its main-beam nulling capability involving mutual coupling. To deal with the mutual coupling, the active element pattern method [14] is adopted. This method utilizes the active pattern of the individual element as the base element to calculate the pattern of a fully excited array, which is more universal than the mutual impedance matrix analysis method [15] without limitation in element type.

The active pattern of the ith element, denoted by $\dot{f}_i(\theta)$, is acquired when only the ith element is excited while all other elements are terminated with match loads. For convenience, all these patterns are obtained in the same coordinate system. Thus, $\dot{f}_i(\theta)$ is a complex pattern, which has absorbed the array's spatial phase term $e^{jkd_i \cos\theta}$ into it. Consequently, the receiving signal and jammer in (1) is modified as (12)

$$S = i_s(t)b_d = i_s(t)\begin{bmatrix} \dot{f}_1(\theta_d) \\ \dot{f}_2(\theta_d) \\ \vdots \\ \dot{f}_N(\theta_d) \end{bmatrix}$$

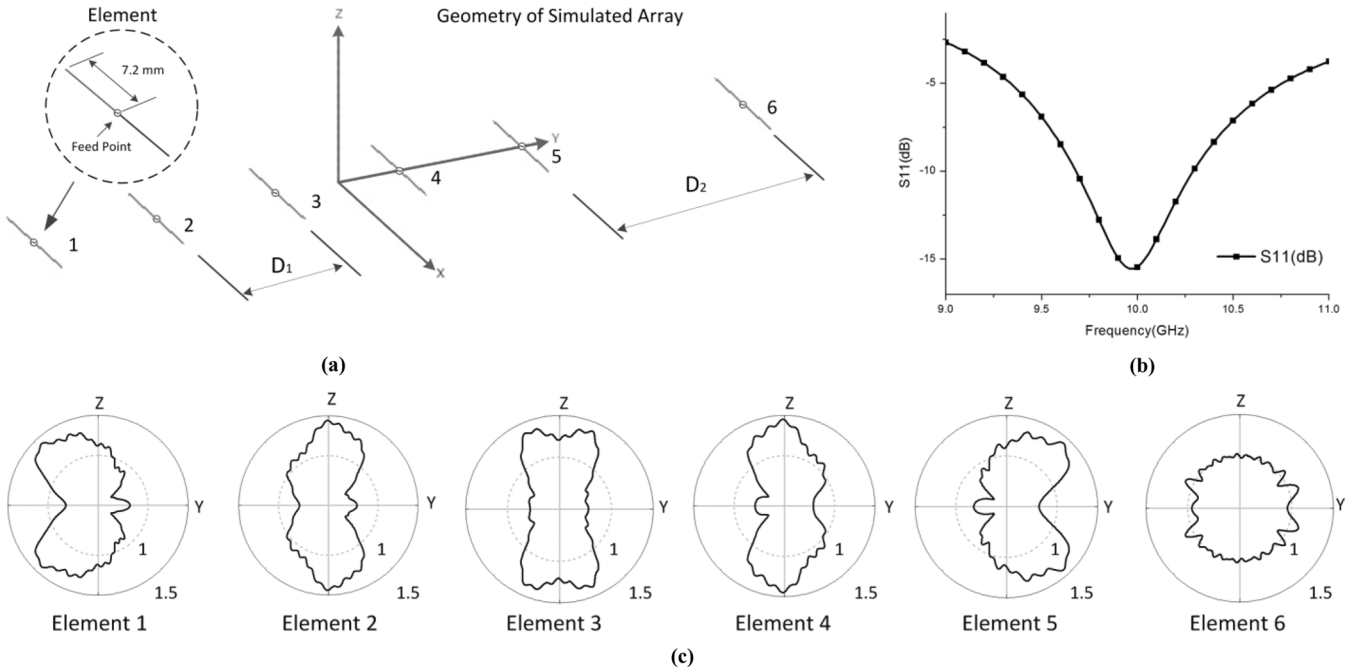

Fig. 9. Simulated dipole array and the character of its elements. (a) Geometry of simulated array. (b) S-parameter of simulated element. (c) Active element patterns.

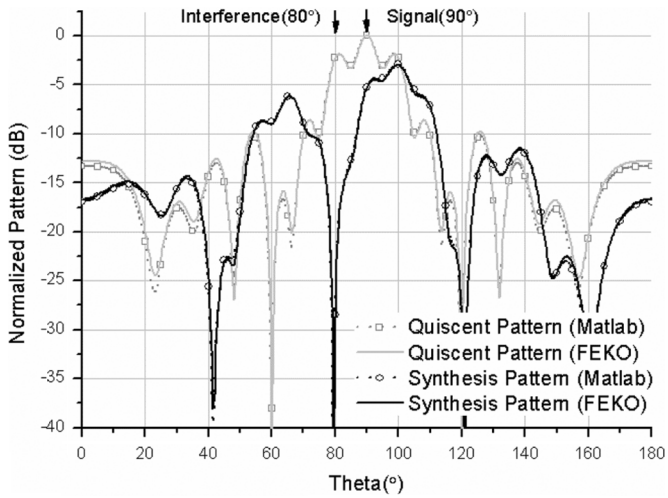

Fig. 10. Comparison between the synthesis pattern generated by numerical analysis tool Matlab and the electromagnetic simulation software FEKO.

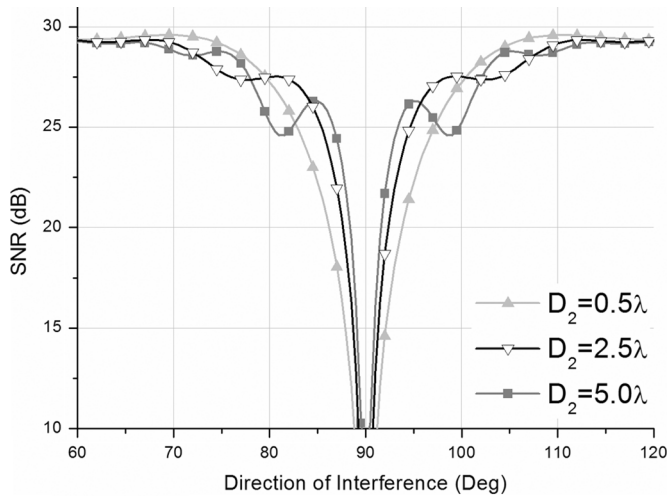

Fig. 11. SNR-θ_j curve at different displacement, $N = 6$ dipole array with mutual coupling.

$$J = i_j(t)b_j = i_j(t)\begin{bmatrix} \dot{f}_1(\theta_j) \\ \dot{f}_2(\theta_j) \\ \vdots \\ \dot{f}_N(\theta_j) \end{bmatrix} \tag{12}$$

and the covariance matrix for the jammer in (2) is replaced as (13), as shown at the bottom of the next page.

Since the noise is not related to the antenna pattern, it is still assumed to be uncorrelated Gaussian white noise with equal variance σ_n, whose covariance matrix can be written as (14)

$$R_{\mathrm{nn}} = \sigma_n^2 \begin{bmatrix} 1 & 0 \\ & \ddots \\ 0 & 1 \end{bmatrix}. \tag{14}$$

With the covariance matrixes (13) and (14), the Applebaum's weighting factor W_{opt} is calculated with (3), and the output SNR is calculated with (10). As for the synthesized pattern of the fully excited array, it can be calculated with (15)

$$f(\theta) = b^T W_{\mathrm{opt}} = \begin{bmatrix} \dot{f}_1(\theta) \\ \dot{f}_2(\theta) \\ \vdots \\ \dot{f}_N(\theta) \end{bmatrix}^T W_{\mathrm{opt}}. \tag{15}$$

Before evaluating the output SNR performance, a six-element dipole array is simulated and compared in both the full-wave simulation software FEKO and numerical analysis tool Matlab to validate the correctness of the calculation method.

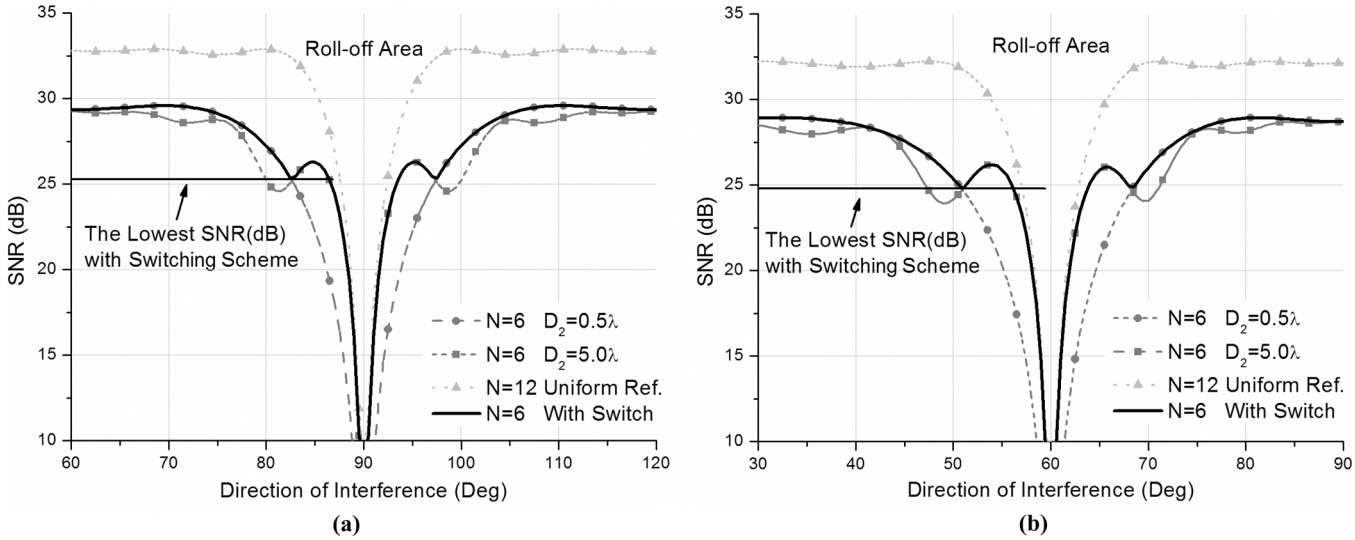

Fig. 12. Performance of the switching scheme with mutual coupling (a) $N = 6, \theta_d = 90^\circ$ (b) $N = 6, \theta_d = 60^\circ$.

The geometry of the array is shown in Fig. 9(a), where five elements are uniformly spaced with $D_1(\lambda/2)$ and one is displaced from others with D_2. The frequency is set at 10 GHz. The S-parameter of the dipole is provided in Fig. 9(b).

In the simulation, the complex active patterns $\dot{f}_i(\theta)$ are exported from FEKO directly. After that, these patterns are normalized with the total radiation power and imported into Matlab to calculate the weighting factors at a presumed interference condition. Finally, a synthesized pattern is generated in Matlab and these weighting factors are assigned back into FEKO to generate a pattern for comparison.

Following this process, the $N = 6, D_2 = 5\lambda$ case is implemented for verification. Active patterns of different elements are shown in Fig. 9(c). Since the sixth element is comparatively far away from other elements, it is less affected by mutual coupling, and its pattern is near isotropic while others are significantly deformed. The presumed direction of interest is set at 90°, and the incident angle of the jammer is set at 80°. The pattern comparison is provided in Fig. 10. It can be found that the synthesis pattern acquired in Matlab matches well with the full-wave simulation result in FEKO, which generates the null in the exact position and validates the correctness of the calculation method.

Finally, the main-beam nulling performance of the proposed scheme involving mutual coupling is studied here again. The input SNR and SIR are set as 20 and -20 dB, respectively, and the output SNR is used to judge the main beam nulling performance.

The relationship between the output SNR and the direction of interference θ_j for $D_2 = 0.5\lambda, D_2 = 2.5\lambda$ and $D_2 = 5\lambda$ cases are plotted in Fig. 11, in which the direction of the signal is set at $\theta_d = 90^\circ$. A steeper roll-off character around the $\theta_j = 90^\circ$ can be observed when D_2 increases, which indicates that this method is still effective when involving mutual coupling. Meanwhile, ripples in the output SNR still exist in these traces when the interference moves away from the main beam region. Therefore, the switching scheme is still required to acquire consistent performance in all regions. Fig. 12 provides the output SNR-θ_j trace for the switching scheme at $\theta_d = 60^\circ$ and $\theta_d = 90^\circ$. A $N = 12$ uniform array is added as a reference, which proves that the switching scheme is still effective and its main-beam nulling performance is comparable to a large scale adaptive array.

VI. Conclusion

In this paper, a novel scheme to improve the main beam nulling performance of the small-scale arrays is proposed and analyzed. This technique uses a displaced element at the end of an adaptive array to improve the output SNR without increasing the system complexity. An analysis of its working mechanism along with detailed simulation results are provided. More than 6 to 12 dB increments in the output SNR can be observed for eight- to four-elements array, respectively. To maintain consistent performance for all nulling regions, a switching scheme is proposed to solve the regional performance deterioration. A switching criterion similar to the selection combining technique is adopted in this scheme, which provides similar main beam nulling performance as a large-scale adaptive array. Moreover, the proposed scheme is examined with a dipole array, which takes the mutual coupling into consideration. The performance enhancement is consistent with the isolated condition, which verifies its feasibility in practice.

$$R_{\mathrm{jj}} = \sigma_j^2 \begin{bmatrix} \dot{f}_1^*(\theta_j)\dot{f}_1(\theta_j) & \dot{f}_1^*(\theta_j)\dot{f}_2(\theta_j) & \cdots & \dot{f}_1^*(\theta_j)\dot{f}_N(\theta_j) \\ \dot{f}_2^*(\theta_j)\dot{f}_1(\theta_j) & \dot{f}_2^*(\theta_j)\dot{f}_2(\theta_j) & \cdots & \dot{f}_2^*(\theta_j)\dot{f}_N(\theta_j) \\ \vdots & \vdots & \ddots & \vdots \\ \dot{f}_N^*(\theta_j)\dot{f}_1(\theta_j) & \dot{f}_N^*(\theta_j)\dot{f}_2(\theta_j) & \cdots & \dot{f}_N^*(\theta_j)\dot{f}_N(\theta_j) \end{bmatrix} \tag{13}$$

ACKNOWLEDGMENT

The authors would like to thank the anonymous reviewers for their valuable comments on Section V and all the suggestions to improve the quality of this paper.

REFERENCES

[1] S. Applebaum, "Adaptive arrays," *IEEE Trans. Antennas Propag.*, vol. 24, no. 5, pp. 585–598, Sep. 1976.
[2] B. Widrow, P. E. Mantey, L. J. Griffiths, and B. B. Goode, "Adaptive antenna systems," *Proc. IEEE*, vol. 55, no. 12, pp. 2143–2159, Dec. 1967.
[3] W. Gabriel, "Using spectral estimation techniques in adaptive processing antenna systems," *IEEE Trans. Antennas Propag.*, vol. 34, no. 3, pp. 291–300, Mar. 1986.
[4] J. Capon, "High-resolution frequency-wavenumber spectrum analysis," *Proc. IEEE*, vol. 57, no. 8, pp. 1408–1418, Aug. 1969.
[5] R. Schmidt, "Multiple emitter location and signal parameter estimation," *IEEE Trans. Antennas Propag.*, vol. 34, no. 3, pp. 276–280, Mar. 1986.
[6] W. Choi, T. K. Sarkar, H. Wang, and E. L. Mokole, "Adaptive processing using real weights based on a direct data domain least squares approach," *IEEE Trans. Antennas Propag.*, vol. 54, no. 1, pp. 182–191, Jan. 2006.
[7] S. T. Smith, "Optimum phase-only adaptive nulling," *IEEE Trans. Signal Process*, vol. 47, no. 7, pp. 1835–1843, Jul. 1999.
[8] J. A. Hejres, "Null steering in phased arrays by controlling the positions of selected elements," *IEEE Trans. Antennas Propag.*, vol. 52, no. 11, pp. 2891–2895, Nov. 2004.
[9] A. Tennant, M. M. Dawoud, and A. P. Anderson, "Array pattern nulling by element position perturbations using a genetic algorithm," *Electron. Lett.*, vol. 30, no. 3, pp. 174–176, Feb. 3, 1994.
[10] L. C. Godara, "Application of antenna arrays to mobile communications. II. Beam-forming and direction-of-arrival considerations," *Proc. IEEE*, vol. 85, no. 8, pp. 1195–1245, Aug. 1997.
[11] B. D. Van Veen, "An analysis of several partially adaptive beamformer designs," *IEEE Trans. Acoust. Speech Signal Process.*, vol. 37, no. 2, pp. 192–203, Feb. 1989.
[12] M. W. Ganz, J. Ward, and B. D. Carlson, "Mainbeam nulling with adaptive array interferometry," in *Proc. 25th Asilomar Conf. Signals, Syst., Comput.*, Nov. 4–6, 1991, vol. 2, pp. 974–978.
[13] J. H. Winters, "Smart antenna techniques and their application to wireless ad hoc networks," *IEEE Wireless Commun.*, vol. 13, no. 4, pp. 77–83, Aug. 2006.
[14] D. F. Kelley and W. L. Stutzman, "Array antenna pattern modeling methods that include mutual coupling effects," *IEEE Trans. Antennas Propag.*, vol. 41, no. 12, pp. 1625–1632, Dec. 1993.
[15] I. Gupta and A. Ksienski, "Effect of mutual coupling on the performance of adaptive arrays," *IEEE Trans. Antennas Propag.*, vol. 31, no. 5, pp. 785–791, Sep. 1983.

Han Wang received the B.S. degree in applied physics from the Beijing University of Posts and Telecommunications, Beijing, China, in 2010. He is currently working toward the Ph.D. degree in electrical engineering from Tsinghua University, Beijing, China.

His current research interests include antenna design and theory, particularly in smart antenna, MIMO antenna, and antenna measurement.

Zhijun Zhang (M'00–SM'04) received the B.S. and M.S. degrees from the University of Electronic Science and Technology of China, in 1992 and 1995, respectively, and the Ph.D. degree from Tsinghua University, Beijing, China, in 1999.

Since August 2007, he has been with Tsinghua University, where he is a Professor with the Department of Electronic Engineering. In 1999, he was a Postdoctoral Fellow with the Department of Electrical Engineering, University of Utah, where he was appointed a Research Assistant Professor in 2001. In May 2002, he was an Assistant Researcher with the University of Hawaii at Manoa, Honolulu, HI, USA. In November 2002, he joined Amphenol T&M Antennas, Vernon Hills, IL, as a Senior Staff Antenna Development Engineer and was then promoted to the position of Antenna Engineer Manager. In 2004, he joined Nokia Inc., San Diego, CA, as a Senior Antenna Design Engineer. In 2006, he joined Apple Inc., Cupertino, CA, USA, as a Senior Antenna Design Engineer and was then promoted to the position of Principal Antenna Engineer. He is the author of *Antenna Design for Mobile Devices* (Wiley, 2011).

Dr. Zhang is serving as an Associate Editor of the IEEE TRANSACTIONS ON ANTENNAS AND PROPAGATION and the IEEE ANTENNAS AND WIRELESS PROPAGATION LETTERS.

Yue Li (S'11–M'12) received the B.S. degree from the Zhejiang University, Zhejiang, China, in 2007, and the Ph.D. degree from Tsinghua University, Beijing, China, in 2012.

Since June 2012, he has been with Tsinghua University, where he is a Postdoctoral Fellow with the Department of Electronic Engineering. He was also a visiting scholar with the Institute for Infocomm Research (I^2R), A*STAR, Singapore, and Hawaii Center of Advanced Communication (HCAC), University of Hawaii, USA. He has authored and coauthored over 30 journal papers, and holds over 10 granted and filed Chinese patents. His current research interests include antenna design and theory, particularly in reconfigurable antennas, mobile/handset antennas, diversity antennas, and antennas in package.

Dr. Li is also serving as a reviewer of the IEEE TRANSACTIONS ON ANTENNAS AND PROPAGATION and the IEEE ANTENNAS AND WIRELESS PROPAGATION LETTERS.

Zhenghe Feng (M'05–SM'08–F'12) received the B.S. degree in radio and electronics from Tsinghua University, Beijing, China, in 1970.

Since 1970, he has been with Tsinghua University, as an Assistant, Lecture, Associate Professor, and Full Professor. His main research areas include numerical techniques and computational electromagnetics, RF and microwave circuits and antenna, wireless communications, smart antenna, and spatial temporal signal processing.